Bifurcation physics of magnetic islands and stochasticity explored by heat pulse propagation studies in toroidal plasmas

Bifurcation physics of magnetic islands and stochasticity explored by heat pulse propagation studies in toroidal plasmas

K. Ida,[1,2] T. Kobayashi,[1] M. Yoshinuma,[1] Y. Suzuki,[1,2] Y. Narushima,[1,2]
T.E. Evans,[3] S. Ohdachi,[1,2] H. Tsuchiya,[1] S. Inagaki,[4] and K. Itoh[1]

[1]*National Institute for Fusion Science, Toki, Gifu 509-5292, Japan*
[2]*The Graduate University for Advanced Studies, 322-6 Oroshi, Toki, Gifu 509-5292, Japan*
[3]*General Atomics, San Diego, California 92186-5608, USA*
[4]*Research Institute for Applied Mechanics, Kyushu Univ., Kasuga, 816-8580, Japan*

(Dated: April 28, 2016)

Bifurcation physics of the magnetic island was investigated using the heat pulse propagation technique produced by the modulation of electron cyclotron heating. There are two types of bifurcation phenomena observed in LHD and DIII-D. One is a bifurcation of the magnetic topology between nested and stochastic fields. The nested state is characterized by the bi-directional (inward and outward) propagation of the heat pulse with slow propagation speed. The stochastic state is characterized by the fast propagation of the heat pulse with electron temperature flattening. The other bifurcation is between magnetic island with larger thermal diffusivity and that with smaller thermal diffusivity. The damping of toroidal flow is observed at the O-point of the magnetic island both in helical plasmas and in tokamak plasmas during a mode locking phase with strong flow shears at the boundary of the magnetic island. Associated with the stochastization of the magnetic field, the abrupt damping of toroidal flow is observed in LHD. The toroidal flow shear shows a linear decay, while the ion temperature gradient shows an exponential decay. This observation suggests that this flow damping is due to the change in the non-diffusive term of momentum transport.

PACS numbers: 52.55.Hc, 52.55.Fa, 52.50.Sw, 52.50.Gj

I. INTRODUCTION

The instability of neoclassical tearing mode has been studied in order to understand the growth and healing of the magnetic island [1–6]. The stabilization of this mode by electron cyclotron heating (ECH) has also been studied to eliminate the magnetic island[7–9]. In helical plasma, usually the neoclassical tearing mode is metastable and the healing of the magnetic island produced by the error field has been observed [10, 11]. The magnetic island is a unique confinement region because it produces a strong poloidal asymmetry of radial heat flux. Most of the heat flux perpendicular to the magnetic field is concentrated to the X-point of the magnetic island. The radial heat flux across the O-point of the magnetic island is significantly reduced and the temperature gradient inside the magnetic island becomes zero or has a small finite value in the high collisional region [12]. Although the temperature profile inside the magnetic island is usually flat (or slightly peaked [13, 14]), there are various experimental observations that suggest good confinement (at least in particle transport of bulk ion and impurity ions) inside magnetic islands [15–17]. The magnetic island has been recognized to play an important role in the formation of the internal transport barrier (ITB), because the foot point of the ITB locates near the rational surface in the steady state phase in tokamak plasmas [18–22], and the transition from L-mode to H-mode phase is observed in the narrow window of rotational transform near the low order rational magnetic surface in helical plasmas [23].

The impact of stochastic magnetic field on electron heat transport has been intensively studied in reverse field pinch (RFP) plasmas, where the magnetic field is usually stochastic [24–28]. In RFP plasmas, good agreement between the electron thermal diffusivity estimated from power balance and the analytic predictions of the Rechester-Rosenbluth model [29] has been reported. However, few papers have been published regarding the impact of stochastic field on electron and ion heat transport and momentum transport in other configurations such as tokamak and helical configuration. This is partly because of a lack of experimental tools to identify the stochastization in tokamak and helical devices. In RFP plasma, the stochastization can be identified by the existence of large magnetic field perturbations with multimode using a large number of magnetic probes located around the vacuum vessel. However, the magnetic fluctuations with higher toroidal and poloidal mode numbers are relatively weak and the transport is governed by the electro-static turbulence rather than the electro-magnetic turbulence in tokamak and helical plasmas.

Heat pulse propagation is a useful tool to investigate the magnetic topology and transport in the toroidal plasma. Recently, the heat pulse propagation has been applied to identify the stochastization of magnetic field in helical and tokamak plasmas. Originally, the heat pulse propagation technique has been used to estimate heat conductivity of plasmas [30–32]. The heat pulse propagation has been recognized to be a powerful tool to study the magnetic topology as well as transport and it is applied to the plasma with magnetic islands or stochastic magnetic field [33]. The heat pulses are produced by the modulation electron cyclotron heating (MECH) with a

frequency of $30 \sim 50$ Hz. The amplitude of the heat pulse, $\delta T_e/T_e$, is derived from the power of Fourier spectrum, $p(f)$, as $\delta T_e/T_e = \sqrt{p(f)\Delta f}$, where f is a frequency of MECH and Δf is a bandwidth of Fourier transform (FFT). The time delay, τ_d, is calculated from the phase delay, $\delta\phi$, as $\tau_d = \delta\phi/(2\pi f)$. In order to analyze the heat pulse propagation in the non-steady state plasma, where the amplitude and phase delay of the heat pulse change rapidly, the wavelet analysis for the heat pulse propagation has been developed [34]. In the wavelet analysis, the amplitude and phase delay are derived from the wavelet transform complex. In this paper, the experimental results of bifurcation phenomena identified by the heat pulse propagation technique in Large Helical Device (LHD) and DIII-D tokamak [35] are described.

II. BIFURCATION OF TOPOLOGY AND TRANSPORT IN MAGNETIC ISLANDS

A. Radial profile of amplitude and delay time of heat pulse

Bifurcation of topology and transport in magnetic islands are observed in LHD and DIII-D plasmas. In LHD experiment, the magnetic field strength is 2.7T with the vacuum magnetic axis of 3.6m and minor radius of 0.6 m. The direction of NBI is changed from co-injection to counter-injection during the discharge. The counter-NBI with 5 MW is to drive the negative plasma current (in the counter-direction) and to decrease the magnetic shear, while the counter-NBI with the power of 1.5 MW is for the MSE measurements. The total plasma current driven by the neutral beam is in the range of -100 kA (counterdirection) to 50 kA (codirection), which is only 3 - 6% of the equivalent plasma current (1.8 MA) produced by the external helical coils. The edge rotational transform decreases due to the NB current drive (NBCD) and the central rotational transform increases due to the inductive current; the magnetic shear at the $\iota/2\pi = 0.5$ (q=2) rational surface starts to decrease and reaches the steady-state value of 0.5 after the switch of the NBI. The line averaged electron density is 1×10^{19} m^{-3} and the central electron temperature is 2 - 3 keV for these three discharges. There is no RMP field applied. The heat deposition of the centrally focused MECH is localized at the magnetic axis within $r_{\rm eff}/a_{99} < 0.1$.

In DIII-D experiment, the poloidal cross section is D-shape with a major radius of 1.7 m and minor radius of 0.6 m for magnetic confinement of high temperature plasmas. The plasma current was 1.3 MA and the toroidal magnetic field is 2 T with an inner wall limiter configuration and a safety factor of $q_{95} = 3.76$. The line-averaged electron density was 3 - 4 $\times 10^{19}$ m^{-3} and the electron temperature in the core region was $\sim$ 2 keV. In this experiment, an $n = 1$ perturbation magnetic field is applied to produce a large $m/n = 2/1$ (m and n are the poloidal and toroidal mode numbers of the island respectively) non-rotating magnetic island at a normalized minor radius $\rho = 0.64$ - 0.8 with the C-coil amplitude of 3.35 kA. A phase flip in the C-coil between 5° and 185° phases is performed. As a result of this phase flip, the X-point and O-point of the magnetic island appears, respectively, at the toroidal angle of electron cyclotron emission (ECE) measurement. The deposition of the modulation electron cyclotron heating (ECH) with a modulation frequency of 50 Hz is focused near the $q = 1$ surface at $\rho = 0.42$ in order to suppress the sawteeth crash.

There are two types of bifurcation phenomena at the magnetic island. One is a bifurcation of magnetic topology between the nested magnetic flux surface and the stochastic magnetic field. The other is a bifurcation of transport between the nested magnetic island with reduced thermal diffusivity and that with extremely reduced thermal diffusivity. The former state is characterized by high accessibility of heat pulses into the magnetic island, while the latter state is characterized by low accessibility of heat pulses into the magnetic island. These two states are called "high" and "low" accessibility magnetic island.

After switching the NBI direction from co-injection to counter-injection, the magnetic shear at the rational surface located at the normalized averaged minor radius of 0.35 decreases due to the decrease of edge rotational transform due to NBCD and the increase of core rotational transform due to the inductive current. When the magnetic shear drops to close to 0.5, the bifurcation of magnetic topology from nested magnetic flux surface to $m/n = 2/1$ magnetic island or to stochastic magnetic field occurs. Whether the magnetic island or the stochastic magnetic field depends on how fast the magnetic shear decreases. The magnetic island appears when the magnetic shear decreases fast ($-ds/dt > 0.25$) in the discharge with lower density, while the stochastic magnetic field appears when the magnetic shear decreases slowly ($-ds/dt < 0.25$) in the discharge with higher density.

The modulation ECH with a frequency of 39 Hz is applied to investigate the change in magnetic topology. The temperature gradient is almost zero even at the nested magnetic flux surface inside the magnetic island because of a lack of radial heat flux across the O-point of the magnetic island. Although the flattening of electron temperature profiles are observed both for the nested magnetic island and the stochastic magnetic field, the radial profiles of the delay time of the heat pulse show significant differences between the nested magnetic island and stochastic magnetic field as seen in Fig.1(a)(b). When the heat pulse propagating from the plasma center reaches the boundary of the magnetic island (at 0.23 and 0.48 of normalized averaged minor radius of $r_{\rm eff}/a_{99}$), it starts to propagate towards the O-point of the magnetic island (outward for $r_{\rm eff}/a_{99} < 0.35$ and inward for $r_{\rm eff}/a_{99} > 0.35$). Here, a_{99} is the effective minor radius in which 99% of the plasma kinetic energy is confined and is 0.63m. Therefore, the radial profile of the delay time shows a clear peak at the O-point of the magnetic

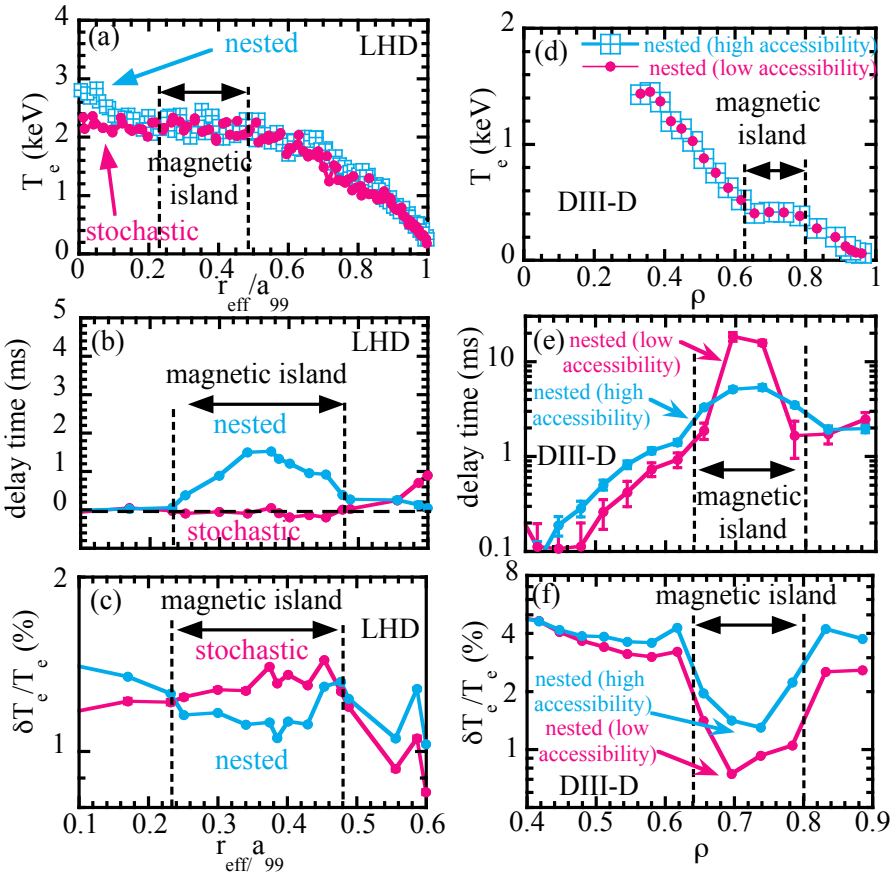

FIG. 1: Radial profiles of (a) electron temperature, (b) delay time, (c) amplitude of heat pulse at the O-point of m/n=2/1 magnetic island with nested flux magnetic flux surface and stochastic magnetic field in LHD plasma, (d) electron temperature, (e) delay time, and (f) amplitude of heat pulse at the O-point of m/n=2/1 magnetic island with low accessibility and high accessibility in DIII-D plasma (From figure 5 in [42] modified).

island [36]. The larger slope of the delay time inside the magnetic island indicates that the thermal diffusivity is lower inside the magnetic island. The reduction of the thermal diffusivity inside the magnetic island observed in this experiment is consistent with the results of the cold pulse propagation experiment [37, 38].

In contrast, when the magnetic field becomes stochastic, the delay time profile shows a flattening because the heat pulse propagates very fast radially along the stochastic magnetic field lines. As seen in Fig.1(c), the reduction of the amplitude of the heat pulse is observed at the O-point of the nested magnetic island. This is because the heat flux across the X-point of the magnetic island becomes more dominant and the heat flux across the O-point of the magnetic island is reduced. The magnetic field perturbation with the lowest mode number (m/n = 2/1) is dominant in the plasma with magnetic islands, while the magnetic field perturbation with higher mode number (m/n = 4/2, 6/3, 8/4) becomes more dominant in the plasma with stochastization [33]. The similar topology bifurcation has also been observed in the spontaneous transition from the stochastic state to helical equilibrium state in reverse field pinch (RFP) plasmas. At the transition, the magnetic field perturbations with multimode in the stochastic state disappears and the magnetic field perturbations with only one single mode becomes dominant [27, 39–41].

In DIII-D, a bifurcation of transport inside m/n=2/1 nested magnetic island was observed. The bifurcation is between a high accessibility states mantic island and a low accessibility states mantic island [42, 43]. Here, an external perturbation coil referred to as the C-coil [44] is used to control the size and phase of the magnetic island. The radial profiles of electron temperature, the delay time, and the amplitude of the heat pulse are plotted in Fig.1(d)(e)(f). The radial profile of electron temperature is identical between these two states within the accuracy and spatial resolution of the measurements. The magnetic island with high accessibility shows the peaked delay time profile which is similar to the nested

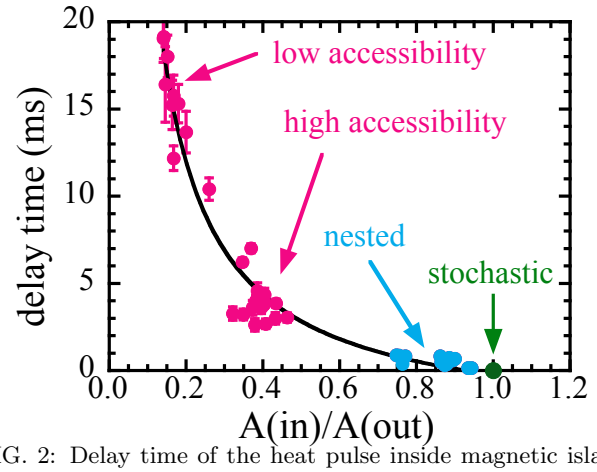

FIG. 2: Delay time of the heat pulse inside magnetic island as a function of the ratio of amplitude inside to outside the magnetic island for the magnetic island with low and high accessibility in DIII-D and the magnetic island with nested flux surface and stochastic magnetic field in LHD.

magnetic island in LHD. In contrast, the magnetic island with low accessibility shows an extremely long delay time of $\sim$ 20 ms, which indicates extremely reduced thermal diffusivity. Because of slow propagation of heat pulse, the amplitude of heat pulses $\delta T_e/T_e$ are reduced significantly inside the magnetic island.

In the two states of a magnetic island, the first state shows low accessibility of the heat pulses and the second state shows high accessibility of the heat pulses appear in one discharge as a self-regulated oscillation with a frequency of 5 Hz in DIII-D during the application of an RMP field. It should be noted that this self-regulated oscillation occurs while the external C-coil perturbation field is held constant in time. Thus, this is represents a spontaneous bifurcation due to a change in plasma response. The self-regulated oscillation occurs when the $m/n = 2/1$ magnetic island is static (not rotating) and its width is relatively large (15% of minor radius) with the balanced NBI where the screening of perturbation field due to the plasma toroidal rotation is small enough.

B. Relation between amplitude and delay time

The reduction of the amplitude of the heat pulse is due to the slower heat pulse propagation inside than outside the magnetic island. The X-point of the magnetic island acts like a bypass of the heat pulse. The relation between the amplitude and the delay time of the heat pulse is studied in the bifurcation phenomena of magnetic topology and transport of magnetic islands in LHD and DIII-D plasmas. Figure 2 shows the delay time as a function of the ratio of the amplitude of the heat pulse inside to that outside the magnetic island. The delay time of the heat pulse is almost zero for the stochastic magnetic field within the accuracy of the measurements ($\sim$ 50 μ sec), which indicates a large effective thermal diffusivity. The effective thermal diffusivity in the stochastic region, χ_{st}, was estimated to be $2 \sim 3 \times 10^2$ m^2/s [33], which is much larger than that in the nested magnetic flux ($\chi_e \sim 4$ m^2/s) by one to two orders of magnitude [45].

In the nested magnetic islands, the delay time is longer (heat pulse propagation becomes slower) and the ratio of the amplitude of the heat pulse inside to that outside the magnetic island becomes smaller. The heat pulse propagation speeds inside magnetic island are 5 times and 40 times slower than that outside the magnetic island for the high accessibility and low accessibility magnetic island, respectively. The slow heat pulse propagation indicates a significant reduction of thermal diffusivity. This observation is consistent with the significant reduction of ion transport inside the magnetic island in JT-60U, where the thermal diffusivity evaluated inside the magnetic island after the back-transition from H-mode to L-mode is $\chi_i = 0.1$ m^2/s and much smaller than that ($\chi_i \sim 1$ m^2/s) outside the magnetic island by an order of magnitude [46].

C. Time scale of transition between two states in the bifurcation phenomena

Time scales of the transition between two states in the bifurcation phenomena of magnetic topology and transport are important parameters in understanding the mechanism of the bifurcation. Figure 3(a)(b) show the contour of the modulation amplitude ($\delta T_e/T_e$) and the delay time (τ_d) of a fundamental component of the heat pulse in space and time in the discharges with forward and backward transitions from magnetic island to stochastic magnetic field and vise-versa in LHD plasmas. Here the running FFT with a time window length of 240ms, which corresponds to six periods of the MECH, and a time shift of 0.5ms was performed to obtain the time evolution of the amplitude and phase delay profiles. The Hanning window was used as the window function, whose half width of the half maximum is 0.5 times the window length. Therefore, the effective time resolution is 120ms that corresponds to 3 periods of the MECH. The transition of topology bifurcation is more clearly observed in the contour of the delay time. The small peak of the delay time at $t = 5.85$ sec and $t = 6.45$ sec indicate the appearance of magnetic inlands, while a large area of small delay time (close to zero) at $t = 5.94$ - 6.32 sec indicate the stochastization of the magnetic field. It is interesting that the region of the stochastic magnetic field shows abrupt expansion at $t = 6.14$ sec as the location of rational surface of $q = 2$ ($\iota/(2\pi) = 0.5$) moves outwards. The outward movement of rational surface is consistent with the jump of magnetic island location from $r_{\rm eff}/a_{99}$ ~ 0.3 (at $t = 5.85$ sec) to $r_{\rm eff}/a_{99} \sim 0.4$ (at $t = 6.45$ sec).

The time scale of the transition is evaluated from the time derivative of the delay time at the transition from

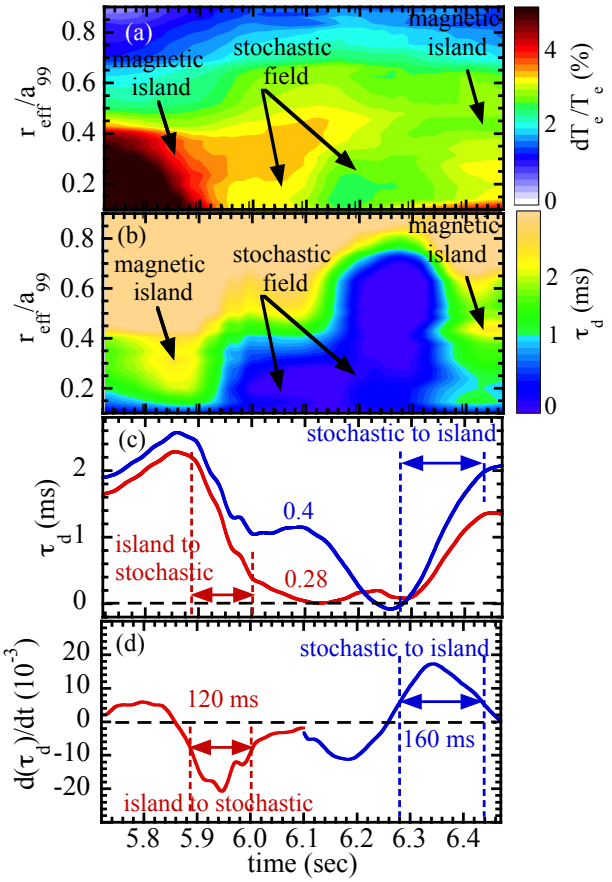

FIG. 3: Contour of (a) temperature modulation amplitude ($\delta T_e/T_e$) and (b) delay time of a fundamental component of a heat pulse in space and time for the discharges with the transition from magnetic island to stochastic magnetic field and stochastic magnetic field to magnetic island, (c) time evolution of the delay time at $r_{\rm eff}/a_{99}$ = 0.28 and 0.4, and (d) time derivative of delay time for the transition from magnetic island to stochastic magnetic field and the transition from stochastic field to magnetic island in LHD plasmas.

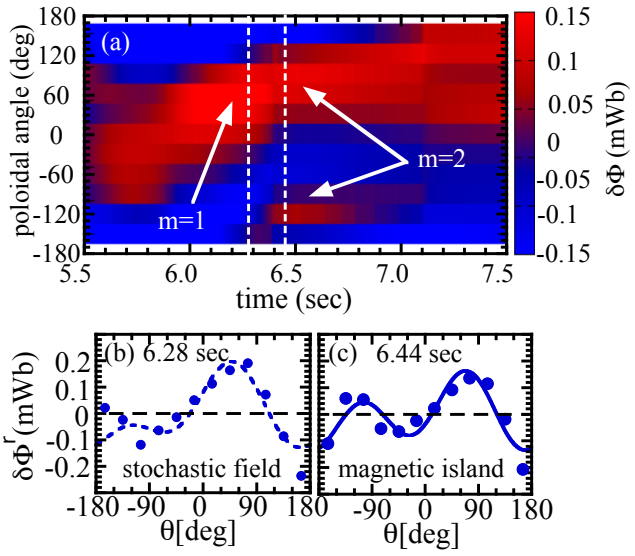

FIG. 4: (a) Contour of amplitude of the perturbation field measured with saddle loop in poloidal angle and time for the discharge plotted in Fig.3 and the poloidal distribution of the perturbation field and the fitted curve with m = 1 and m = 2 Fourier component at (b) t = 6.28 sec (stochastic magnetic field) and (c) 6.44 sec (magnetic island) in LHD plasmas.

magnetic island to stochastic field (t = 5.95 sec) and the transition from magnetic island to stochastic field (t = 6.35 sec) as seen in Fig.3(c)(d). The transition time defined by the 1/e width of the peak of time derivative delay time ($d\tau_d/dt$) are 120 ms and 160 ms for the transition from magnetic island to stochastic field and vise-versa, respectively. This is not the time scale of local stochastization of magnetic field at the rational surface but the time scale of radial expansion of the stochastic region from the rational surface to the magnetic axis as seen in the radial propagation of the onset time of the flow damping [47]. Therefore, the transition time scale from magnetic island to stochastic field discussed here is determined by the speed of radial expansion of the stochastic region from the rational surface to the magnetic axis and depends on the change in $\iota/(2\pi)$ profiles.

In general, the magnetic perturbation field of m/n = 1/1 magnetic island can be easily detected by the poloidal array of the saddle loop in LHD. When the size of the m/n = 2/1 magnetic island becomes large, the m = 2 component overlaps to the m = 1 component of the magnetic perturbation field. Figure 4(a) shows the contour of amplitude of the perturbation field measured with saddle loop in poloidal angle and time for the discharge plotted in Fig.3. The peak of the magnetic perturbation field shifts from - 30 degree to +90 degree in time due to a slow phase shift of the m/n = 1/1 magnetic island[48]. At the transition from stochastic field to magnetic island (t = 6.4 sec), the m = 2 component of the magnetic perturbation field suddenly appears. Then the m = 2 component becomes weak and finally disappears at t = 7.0 sec. As seen in Fig4(b)(c), the poloidal distribution of the perturbation field before the transition from stochastic field to magnetic island (t = 6.28 sec) shows m = 1 component due to the m/n = 1/1 magnetic island near the plasma periphery ($r_{\rm eff}/a_{99} \sim 0.9$) and there is no clear m = 2 component due to the m/n = 2/1 magnetic island observed. In contrast, after the transition from stochastic field to magnetic island (t = 6.44 sec), m = 2 component due to the m/n = 2/1 magnetic island located in the plasma core ($r_{\rm eff}/a_{99} \sim 0.4$) becomes significant and even larger than the m = 1 component due to the m/n = 1/1 magnetic island near the plasma periphery. The change in poloidal distribution of the perturbation field at the transition is consistent with the change in delay

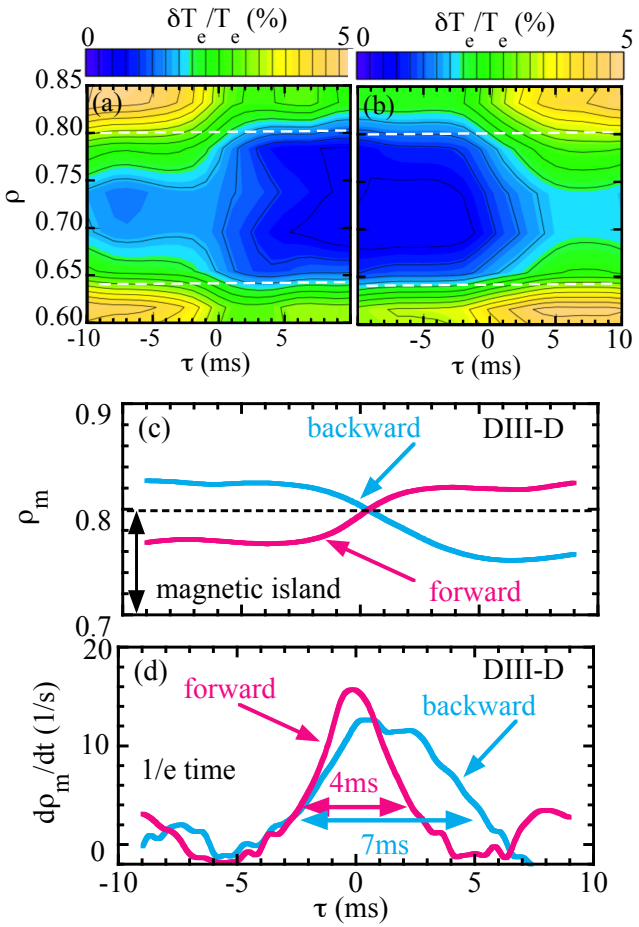

FIG. 5: Contour of relative modulation amplitude of electron temperature in space and time during the (a) forward transition (from high accessibility to low accessibility magnetic island) and (b) backward transition (from low accessibility to high accessibility magnetic island) at O-point (From figure 6 in [42]) and the time evolution of (c) outer normalized minor radius of the heat pulse penetration, and (d) time derivative of the normalized minor radius for the forward (high to low accessibility) and backward (low to high accessibility) transition in DIII-D plasmas. The white dashed lines indicate the region of the magnetic island.

time profiles evaluated from heat pulse propagation.

In contrast, the transition between two states of transport inside the magnetic island observed in DIII-D is much faster than the transition of magnetic topology. Because the transition time scale is even smaller than one period of the modulation of ECH, it is difficult to evaluate the transition time from the delay time but can be estimated from the amplitude of heat pulse. The time evolution of the temperature perturbation amplitude was obtained with the rectangular windowed running FFT having a time window length of 20ms, which corresponds to one period of the MECH, and a time shift of 1 ms. Note that the edge discontinuity of each FFT window was negligibly small, since the temperature perturbation amplitude was sufficiently larger than the noise amplitude and the slow drift of the mean temperature. Figure 5(a)(b) show the contour of modulation amplitude ($\delta T_e/T_e$) near the magnetic island (ρ = 0.64 - 0.8) for the forward transition (from high accessibility to low accessibility) and backward (from low accessibility to high accessibility) transition in DIII-D plasmas. In the high accessibility magnetic island, the heat pulse penetrates into the magnetic island, while the penetration of the heat pulse is suppressed in the low accessibility magnetic island. The time evolutions of the normalized minor radius (ρ_m) with equal modulation amplitude and their time derivative are plotted in Fig.5(c)(d) for the forward and backward transitions. The transition time defined by the 1/e width of the peak of time derivative delay time ($d\rho_m/dt$) is 4 ms and 7 ms for the forward and backward transition of transport in the magnetic island, respectively. The time scale of the transition of transport observed in DIII-D is much shorter than that of the magnetic topology observed in LHD plasmas.

The difference of mechanism in the topology bifurcation in LHD and the transport bifurcation is discussed. Time derivative of the width of magnetic island, W, normalized by minor radius of magnetic island, r_s, is determined by 1) the neoclassical tearing instability, 2) the bootstrap current near the O-point of the island, and 3) the ion-polarization current effect, and can be expressed by the Rutherford equation (e.g., [49]) as

$$\tau_R \frac{\partial (W/r_s)}{\partial t} = \Delta^{'} r_s + \alpha \frac{\sqrt{\epsilon}\beta_p^{'}(W/r_s)}{(W_c/r_s)^2 + (W/r_s)^2} + g\frac{(V_*/V_H)^2}{(W/\tau_s)^3} \quad (1)$$

and

$$\Delta^{'} = \Delta_0^{'}(1 - \delta^2/W^2) \quad (2)$$

where $\Delta_0^{'}$ is the tearing-stability parameter and δ is the island width due to the vacuum external magnetic field, indicating the induction of the magnetic island produced by external coil [50, 51]. Here, W_c denotes the critical width of island and is determined by the competition between parallel thermal conductivity and perpendicular thermal conductivity given in [52] as,

$$\frac{W_c}{\tau_s} \sim \left(\frac{\chi_\perp}{\epsilon^2 \chi_\parallel}\right)^{1/4}. \quad (3)$$

$\chi_\perp$, is the perpendicular thermal diffusely inside the magnetic island and is determined by the turbulence which is penetrated from outside the magnetic island by turbulence spreading [53, 54]. If the perpendicular thermal diffusivity is large, the finite temperature gradient penetrates into the island, so that the Bootstrap current remains in the island, making the island thinner.

The time scale for the stochastization evaluated by the growth of flattening region of the electron temperature profile is $\sim$ 50 ms [55]. The time scale of the topology bifurcation and growth of island width, W, observed in LHD is consistent with that predicted by the Rutherford equation above, because the growth rate of the magnetic island is accelerated by $(2|\Delta'_0|r_s/W_c) \approx 10^2$ compared with τ_R (2 - 3 sec) in this experiment. In contrast, the transition between the low accessibility and high accessibility magnetic islands in DIII-D plasmas is due to the bifurcation of the critical width of island of W_c which is determined by the rapid change in perpendicular thermal diffusivity.

III. PLASMA FLOW AT MAGNETIC ISLANDS

It is well known that the size of the magnetic island is sensitive to the plasma rotation because of the shielding of perturbation field externally applied. When the width of the magnetic island becomes large, the mode locking and stooping of the plasma rotation occurs. Therefore the plasma rotation is one of the key plasma parameter in the feedback process of growing/suppression the magnetic island and may contribute the bifurcation of the magnetic topology. In this paper the impact of magnetic islands and stochasticity on momentum transport is discussed. The impact of magnetic island on the momentum transport is different from the heat transport because the perturbation of the magnetic field has a direct influence on plasma flow. The damping of poloidal flow at the magnetic island was observed in LHD [56]. The damping of toroidal flow has been commonly observed as mode locking in tokamak plasmas and as a response of resonant magnetic perturbation (RMP) field in tokamak and helical plasmas.

Figure 6 shows the radial profiles of toroidal rotation velocity during the scan of toroidal torque in time (co-injection to counter-injection) in the RMP experiment in LHD and the mode locking phase in JT-60U [46, 57]. When there is no RMP field ($I_{\rm RMP} = 0$A), the toroidal rotation velocity in the core region ($r_{\rm eff}/a_{99} < 1$) changes as the direction of toroidal torque by the neutral beam injection (NBI) is reversed from co- to counter-direction as seen in Fig.6(a). The direction of core ($r_{\rm eff}/a_{99} < 0.7$) rotation is parallel to the direction of toroidal torque of NBI, while there is offset of toroidal rotation velocity due to the intrinsic torque in the counter direction in the plasma [58, 59]. However, when the RMP field is applied, the toroidal rotation velocity inside the O-point of the magnetic island is unchanged regardless of the direction of toroidal torque. It is interesting that the X-point of the magnetic island acts like a pivot point of toroidal rotation velocity, where the counter-rotation increases on the inner side of the X-point $r_{\rm eff}/a_{99} < 0.94$, while it decreases on the outer side of the X-point $r_{\rm eff}/a_{99} > 0.94$.

In contrast, the magnetic islands are usually rotating in tokamak plasma. When the magnetic island becomes

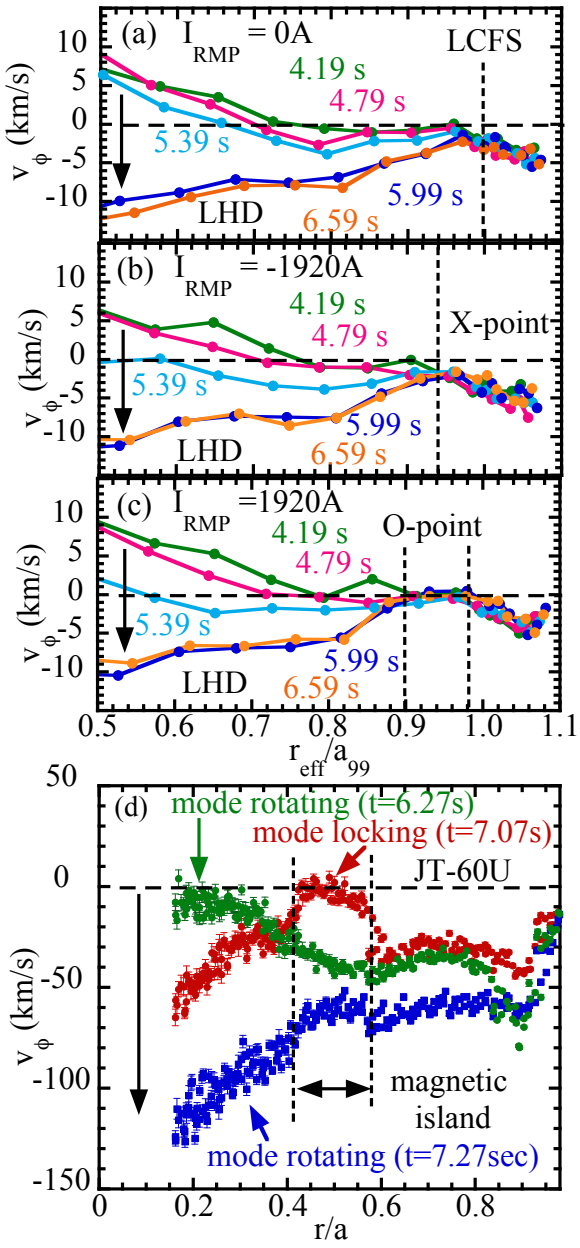

FIG. 6: Radial profiles of toroidal rotation velocity in the LHD plasmas at t = 4.19, 4.79, 5.39, 5.99, and 6.59 sec after the switch of the beam from co-injection to counter-injection at t = 5.3 sec (a) without resonance magnetic perturbation (RMP) field, (b) X-point and (c) O-point in the plasma with RMP, and (d) during mode locking phase and mode rotating phase in the JT-60U plasmas.

large enough with the low toroidal rotation, the mode locking takes place. Then the toroidal rotation velocity inside the magnetic island becomes zero, while there is significant rotation velocity outside the magnetic island as seen in toroidal rotation velocity profiles at the mode locking phase in Fig.6(d). The damping of toroidal ro-

tation velocity inside the magnetic island produces the large velocity shear at the boundary of the magnetic island, which may contribute to the reduction turbulence and the thermal diffusivity at the boundary of the magnetic island. Then, the suppression of turbulence at the boundary of the magnetic island contributes to the improvement of momentum transport (reduction of viscosity) and hence the further increase of velocity shear. This complex interplay between transport and velocity shear is one of the candidates of the reduction of turbulence-driven transport in the proximity of rational surfaces [60]. When the mode is rotating, the toroidal rotation inside the magnetic island becomes finite and large velocity shear at the boundary of the magnetic island disappears.

IV. STOCHASTIC MAGNETIC FIELD

When the size of the magnetic island reaches a critical value, magnetic braiding or appearance of the secondary magnetic island can occur. The phenomena has been predicted theoretically [61] and also observed in experiment [62]. The stochastization of the magnetic field in the core plasma can trigger a major disruption in the tokamak plasmas [63, 64] while the stochastization of the magnetic field in the edge region may enhance the edge transport and contribute to the mitigation of edge localized mode (EML) in the RMP experiment [65, 66]. It is one of the important issues whether the magnetic field becomes stochastic or nested when the RMP field is applied to the plasma for ELM suppression. The heat pulse propagation method is considered to be a powerful tool to identify the magnetic topology in RMP experiments.

A. Stochastization in plasma core

Large stochastization of the magnetic field has been observed in LHD. The stochastization of the magnetic field starts from the rational surface of q = 2 located at half of the plasma minor radius and the stochastic magnetic field region can extend to the magnetic axis. Even though the magnetic field in the large region in the core plasma $r_{\rm eff}/a_{99} < 0.6$ becomes stochastic due to the overlapping of magnetic fields with fundamental and higher harmonic mode, there is no major disruption because the poloidal field is produced by the external coil current, not the plasma current inside.

Figure 7 shows the Poincaré map of magnetic field line for stochastic magnetic field and nested magnetic flux surface and radial profiles of (b) electron temperature, (c) delay time, and (d) amplitude of the heat pulse for nested magnetic field and stochastic magnetic field. Poincare map of magnetic field lines in the plasmas with a magnetic island and stochastic region calculated by an 3D equilibrium code (HINT[67]) and a magnetic field tracing code (MGTRC[68]) with a perturbation magnetic field consistent with the measured iota profile and poloidal

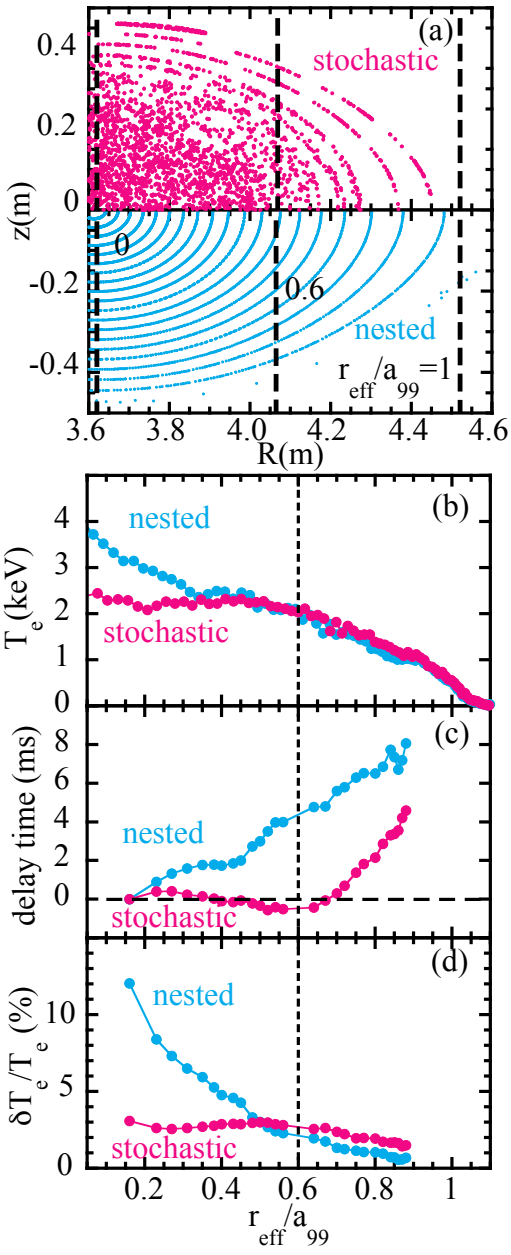

FIG. 7: (a) Poincaré map of magnetic field line for stochastic magnetic field and nested magnetic flux surface and radial profiles of (b) electron temperature, (c) delay time, and (d) amplitude of the heat pulse for nested magnetic field and stochastic magnetic field.

distribution of the perturbed radial magnetic field. The pressure and current profiles, which give a consistent magnetic axis shift evaluated from the radial profile of electron temperature measured with YAG Thomson scattering and rotational transform measured with MSE are used in the 3D equilibrium calculation. The higher harmonic perturbation toroidal currents with the mode num-

bers of $m/n = 4/2$, 6/3, and 8/4 in addition to the lowest mode number of $m/n = 2/1$ are added at the rational surface ($\iota/2\pi = 0.5$) to reproduce the stochastic magnetic field.

The major radius of plasma center ($r_{\rm eff}/a_{99} = 0$), outer location of stochastic magnetic field ($r_{\rm eff}/a_{99} = 0.6$), and the plasma edge ($r_{\rm eff}/a_{99} = 1$) are 3.62 m, 4.07 m, and 4.52 m, respectively. Because the power deposition of the modulation electron cyclotron heating (ECH) is localized near the magnetic axis ($r_{\rm eff}/a_{99} < 0.1$), the electron temperature profile is peaked at the plasma center, the amplitude of the modulation is very peaked near the magnetic axis, and the heat pulse propagates radially towards the plasma edge in the time scale of transport in the plasma with nested magnetic field. The modulation amplitude exceeds 10 % of the mean value near the magnetic axis and decreases monotonically to the level below 1 %. When the magnetic field becomes stochastic the flattening of mean electron temperature, delay time, and amplitude of heat pulse propagation are observed. This is due to the fast heat pulse propagation along the magnetic field which deviates radially from the original nested magnetic flux surface. The region of the stochastic magnetic field can be determined by the region where the time delay of the heat pulse is almost zero within the accuracy of this measurement. Since the deposited power of ECH spreads quickly radially along the stochastic magnetic field, the modulation amplitude drops to only 3 % when the magnetic field becomes stochastic.

B. Stochastization near the plasma periphery

Because of the non-axisymmetric magnetic field, the region with stochastic magnetic field always exists at the periphery of LHD plasmas [69] and there is no strong ELM activity in the H-mode plasma in LHD. The RMP field is used to investigate the effect of RMP field on magnetic topology and transport in the plasma. In order to investigate whether the RMP field can cause the stochastization of the magnetic field, the RMP field is applied to the configuration with $R_{\rm ax}$=3.6 m and with quadruple magnetic field component $B_{\rm Q}$=72 %. By decreasing the quadruple magnetic field component $B_{\rm Q}$ from 100% (standard configuration) to 72 %, the flux averaged poloidal cross section is elongated vertically, with a slight decrease of effective minor radius, a_{99}, from 0.63m to 0.62m.

In this configuration, small vacuum magnetic islands with the poloidal and toroidal mode of $m/n = 8/10$ and $m/n = 6/10$ appear near the plasma edge at $R = 4.46$m and $R = 4.535$m as seen in the Poincaré map of magnetic field line in Fig.8(a). The temperature flattening is observed in the $m/n = 8/10$ magnetic island located at $R = 4.46$m. As the RMP current is increased from 100 to 300A, the connection length between two magnetic islands ($R \sim 4.5$m) decreases due to the stochastization of magnetic field and the location of the flattening moves outwards and the size of the temperature flattening also increases from 3 cm to 5 cm as seen in Fig.8(b). As seen in Fig.8(c), the delay time becomes almost zero (decreases to the level of uncertainty) as the RMP current is increased to 300 A, which indicates that the magnetic field becomes stochastic. The size of the magnetic island in this experiment is only 3 cm and too small to resolve the peak profile of delay time. Fig.8(d) shows the ra-

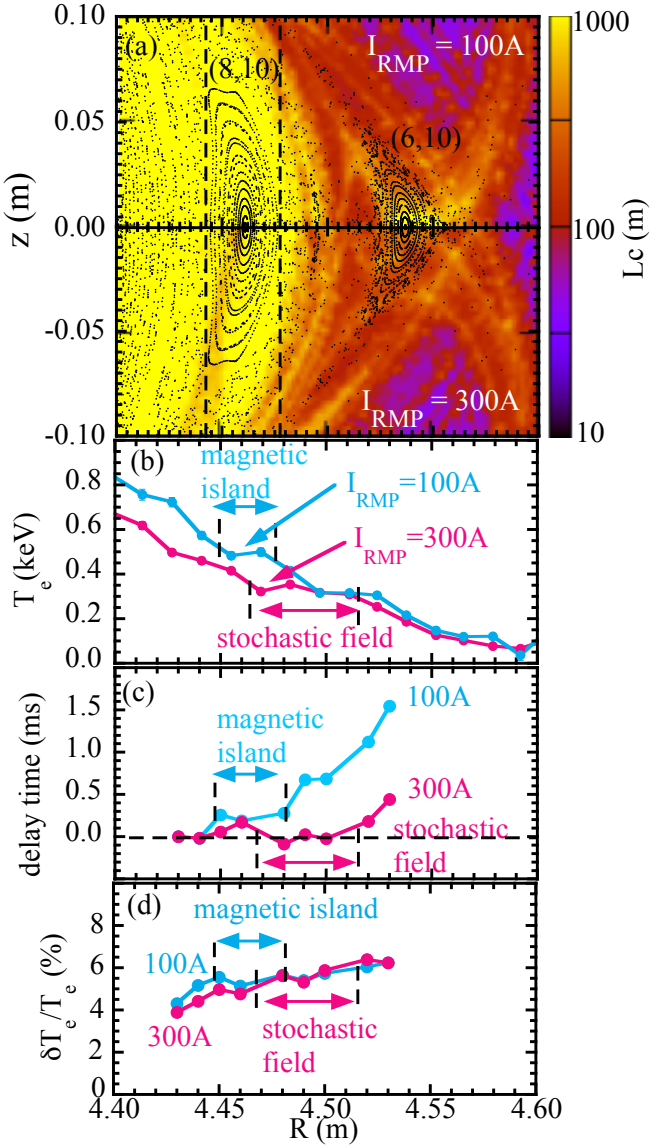

FIG. 8: (a) Poincaré map of magnetic field line in vacuum field with intrinsic $m/n = 8/10$ and $m/n = 6/10$ magnetic islands without resonance magnetic perturbation (RMP) field and color contour of connection length with RMP (100A and 300A) and radial profiles of (b) electron temperature, (c) delay time, and (d) amplitude of the heat pulse near the plasma periphery with RMP coil current of 100 A and 300 A, respectively.

dial profile of the relative amplitude of the heat pulse. The relative amplitudes are ~ 5 % and larger than that in the plasma core and the relative amplitude increases in radius because of the decrease of mean temperature. The radial profile of the relative amplitude of heat pulse is flat even in the nested magnetic field. This is because the increase of flux surface (which causes decrease of the amplitude of the heat pulse) becomes smaller near the plasma edge. Therefore the change in relative amplitude of the heat pulse due to the stochastization is not clearly observed near the plasma edge.

The mode number of RMP field applied is $m/n = 1/1$ and different from the mode number of original vacuum magnetic islands of $m/n = 8/10$ and $m/n = 6/10$. Because the width of $m/n = 8/10$ magnetic island is 3 cm, which is much smaller than that of $m/n = 2/1$ magnetic island (15 cm) plotted in Fig.1, the bump of the delay time can not be observed. However, when the $m/n = 1/1$ RMP field is increased to 300 kA, the magnetic field becomes stochastic due to the overlapping of $m/n = 8/10$ and $m/n = 1/1$ magnetic island near $\iota/(2\pi) = 1$ rational surface and the stochastic region is expanded to 5 cm. In this experiment, the flattening in both the electron temperature and the delay time of the heat pulse are observed, which is clear evidence of the stochastization of the magnetic field.

In general, the magnetic topology can be modified significantly from the magnetic field structure produced by the overlapping of the equilibrium magnetic field and the vacuum perturbed magnetic field due to RMP because of the response of the plasma [70]. For example, the magnetic island can be easily healed by the screening effect due to the plasma rotation. Therefore, the experimental evidence for the stochastization of the magnetic field is indispensable in RMP experiment. This heat pulse propagation experiment in LHD demonstrates that the heat pulse propagation is a very powerful tool to identify magnetic topology, whether the magnetic field becomes stochastic or not, in the RMP experiment in toroidal plasmas.

V. FLOW DAMPING DUE TO STOCHASTIC MAGNETIC FIELD

Since the magnetic islands cause damping of plasma flow, the stochastic magnetic field due to the overlapping of magnetic islands should also have a strong impact on plasma flow. The response of the toroidal rotation velocity to the stochastization of the magnetic field is studied in LHD. Figure 9 shows the radial profiles of electron temperature, electron density, ion temperature, and toroidal rotation velocity in counter-direction (negative sign) for the plasma with nested magnetic field and stochastic magnetic field. Both electron and ion temperature profiles show the core flattening due to the stochastization of the magnetic field as seen in Fig.9(a)(c). It is important that there is a difference in the flattening (gradient of temperature in the stochastic region) between ion and electron temperature profiles.

The thermal diffusivity in the stochastic region can be evaluated as $\chi^{st}_{i,e} = D_M v_{e,i}$, where v_e and v_i are the thermal velocities of electrons and ions, respectively, and D_M is the diffusion of the field line defined in [45, 71, 72]. Therefore, the effective thermal diffusivity in the stochastic magnetic field is proportional to the thermal velocity of particles and the difference in the magnitude of the flattening between ion and electron temperature profiles is due to the difference in thermal velocity of ions and electrons. The core region of the electron density profile is flat even in the plasma with nested magnetic field and the change in the density profile associated with the bifurcation from nested to stochastic magnetic field is small as seen in Fig.9(b). The core toroidal rotation velocity drops significantly in the plasma with stochastic magnetic field as seen in Fig.9(d). The drop of toroidal rotation velocity starts at the rational surface of $\iota/(2\pi) = 0.5$ and expands to the magnetic axis in the time scale of 40ms [42].

The flow damping observed cannot be explained by the simple Rechester-Rosenbluth model [29], because the increase of Prandtl number observed associated with the stochastization is 3 and much larger than that predicted ($\sim$1) and there are clear differences in the decay between ion temperature and toroidal flow velocity [47]. The toroidal flow shear shows a linear decay, while the ion temperature gradient shows an exponential decay. These results suggest that the damping of flow is due to the change in the non-diffusive term of momentum transport or a direct electromagnetic effect associated with the stochastization of the magnetic field[59, 73, 74].

The flow damping due to the stochastization of magnetic field is an important finding, because this experimental result implies the damping of poloidal mean and zonal flow may increase the H-mode threshold power when the RMP is applied to the tokamak plasma. It is important to investigate experimentally how the poloidal mean and zonal flow are affected by the change of magnetic topology, such as the appearances of magnetic island and stochastic magnetic field to predict the H-mode power threshold in ITER. Furthermore the flow damping mechanism observed in this experiment should give a hint in understanding the time scale of magnetic field reconnection in the solar flare[75–77].

VI. DISCUSSION

In this paper, the amplitude and phase delay (delay time) of the fundamental component of the modulation frequency of MECH are analyzed and higher harmonic components of the heat pulse are not taken into account. However, the propagation of the higher harmonic component of the heat pulse is quite different from that of the fundamental component of the heat pulse because of the existence of non-local transport in the toroidal plas-

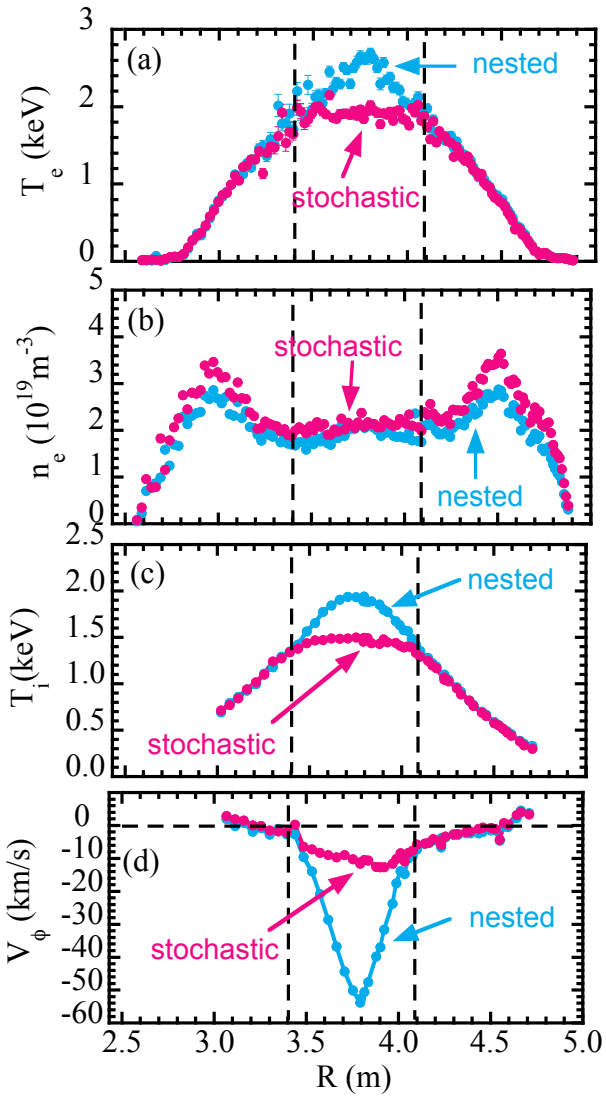

FIG. 9: Radial profiles of (a) electron temperature, (b) electron density, (c) ion temperature, and (d) toroidal rotation velocity in the plasma with nested and stochastic magnetic fields. The dashed lines indicate the region where the stochastization of magnetic field occurs in LHD.

mas [78]. For example, the higher harmonic component of the heat pulse propagates radially much faster than that of fundamental component [79, 80]. It is also found that the higher harmonic component of the heat pulse has a much longer decay length than that predicted by the diffusive model [81]. The hysteresis in the flux gradient relation appears clearly when the perturbation of the heat pulse (product of heating power and pulse width of the MECH) becomes large [82].

The higher harmonic component of the heat pulse is neglected in this study. Since the higher harmonic component propagates faster with longer decay length than the fundamental component, it may produce the apparent fast propagation or even negative propagation near the plasma periphery, where the fraction of the higher harmonic component becomes larger due to the longer decay length. In this case, the fundamental component does not catch the property of heat pulse propagation. The higher harmonics should be evaluated precisely to characterize the heat pulse propagation. Uncertainty of evaluation of the higher harmonics is large compared to that of the fundamental component because the perturbation of the electron temperature is usually small. Thus the conditional averaging technique should be necessary to increase the noise to signal ratio of the electron cyclotron emission (ECE) signal.

In summary, the bifurcation physics of the magnetic island was investigated by the heat pulse propagation technique produced by the modulation electron cyclotron heating. There are two types of bifurcation phenomena observed in LHD and DIII-D. One is a bifurcation of the magnetic topology between the nested and the stochastic field. The former state is characterized by the bi-directional (inward and outward) propagation of the heat pulse with slow propagation speed. The latter state is characterized by the fast propagation of the heat pulse with electron temperature flattening. The other is a bifurcation of the transport in the magnetic island with larger thermal diffusivity and smaller thermal diffusivity. In both cases, the bi-directional (inward and outward in radius) propagation of the heat pulse is observed. In the state of lower thermal diffusivity, the propagation of the heat pulse is extremely slow (40 times slower than that outside magnetic islands).

The time scale of the transition between these two states is quite different in these two bifurcation phenomena. The transition of the magnetic topology bifurcation is relatively slow (50 $\sim$ 150ms) because the change in toroidal current is necessary in this bifurcation. In contrast, the transition of the transport bifurcation is fast (4 $\sim$ 7ms) because only change in the turbulence penetration length into the magnetic island (only the change in the critical island width W_c not the actual island width W) is necessary.

The damping of toroidal flow is observed at the O-point of the magnetic island both in helical and tokamak plasmas. In tokamak, magnetic island can rotate but the local flow damping inside the magnetic island and hence the strong flow shears are observed at the boundary of the magnetic island when the mode locking occurs. Associated with the stochastization of the magnetic field, the abrupt damping of toroidal flow is observed in LHD. This flow damping in the stochastic magnetic field is stronger than that predicted by the Rechester-Rosenbluth model, which suggests the additional damping mechanism of flow. The toroidal flow shear shows a linear decay, while the ion temperature gradient shows an exponential decay. This observation suggests that the flow damping is due to the change in the non-diffusive term of momentum transport.

The authors would like to thank the technical staff of

the LHD, DIII-D, and JT-60U for their support of these experiments. This work is supported by NIFS/NINS under the project of Formation of International Scientific Base and Network and Grant-in-Aid for Scientific Research (No. 15H02336, 21224014, 23360414, 23246164) of JSPS Japan. This work is supported by NIFS/NINS under the project of Formation of International Scientific Base and Network (KEIN1111, KEIN1113). This work is also supported in part by the collaboration program of RIAM Kyushu University and of the National Institute for Fusion Science (NIFS13KOCT001), and by the United States Department of Energy under DE-FC02-04ER54698, DE-FG03-97ER54415 & DE-AC05-00OR22725.

[1] Chang, Z., *et al.* 1995 *Phys. Rev. Lett.* **74** 4663.
[2] Sauter, O., *et al.* 1997 *Phys. Plasmas* **4** 1654.
[3] La Haye, R.J. and Sauter, O. *et al.* 1998 *Nucl. Fusion* **38**, 987.
[4] Buttery, R.J., *et al.* 2002 *Phys. Rev. Lett.* **88** 125005.
[5] Zohm, H., *et al.* 1997 *Phys. Plasmas* **4**, 3433.
[6] Isayama, A., *et al.* 2009 *Nucl. Fusion* **49** 055006.
[7] Isayama, A., *et al.* 2003 *Nucl. Fusion* **43** 1272.
[8] Petty, C.C., *et al.* 2004 *Nucl. Fusion* **44** 243.
[9] Classen, I.G.J., *et al.* 2007 *Phys. Rev. Lett.* **98** 035001.
[10] Narihara, K., *et al.* 2001 *Phys. Rev. Lett.* **87** 135002.
[11] Ohyabu, N., *et al.* 2002 *Phys. Rev. Lett.* **88** 055005.
[12] van Milligen, B., *et al.* 1993 *Nucl. Fusion* **33** 1119.
[13] de Vries, P.C., *et al.* 1997 *Plasma Phys. Control. Fusion* **39** 439.
[14] Stephens, H.D., 2010 *Phys. Plasmas* **17** 056115.
[15] Ida, K., Fonck, R.J., Hulse, R.A., and Leblanc, B., 1986 *Plasma Phys. Controlled Fusion* **28** 879.
[16] Weller, A., *et al.*., 1987 *Phys. Rev. Lett.* **59** 2303.
[17] deVries, P.C., Waidmann, G., Krämer-Flecken, A., Donné, A.J.H., and Schüller, F.C.,1997 *Nucl. Fusion* **37** 1641.
[18] Koide, Y., *et al.* Phys. Rev. Lett. **72** 3662 (1994).
[19] Joffrin, E., *et al.* Nucl. Fusion **43** 1167 (2003).
[20] Estrada, T., *et al.* Nucl. Fusion **47** 305 (2007).
[21] Hidalgo, C., *et al.* Plasma Phys. Control. Fusion **42** A153 (2000).
[22] Ida, K., *et al.* 2009 *Nucl. Fusion* **49** 095024.
[23] Hirsch, M., *et al.* 2000 *Plasma Phys. Control. Fusion* **42** A231.
[24] Bartiromo, R. *et al.* 1999. *Phys. Rev. Lett.* **82**, 1462.
[25] Innocente, P. *et al.* 2007 *Nucl. Fusion* **47**, 1092.
[26] Biewer, T.M. *et al.* 2003 *Phys. Rev. Lett.* **91**, 045004.
[27] Sarff, J.S., *et al.* 2003 *Nucl. Fusion* **43** 1684 (2003).
[28] Fiksel, G. *et al.* 1996 *Plasma Phys. Control. Fusion* **38**, A213-A225 (1996).
[29] Rechester, A.B. and Rosenbluth, M.N. 1978 *Phys. Rev. Lett.* **40** 38.
[30] Lopes Cardozo, N.J., 1995 *et al. Plasma Phys. Control. Fusion* **37**, 799.
[31] Stroth, U., 1996 *et al. Plasma Phys. Control. Fusion* **38**, 611.
[32] Ryter, F., 2010 *et al. Plasma Phys. Control. Fusion* **52**, 124043.
[33] Ida, K., *et al.* 2013 *New J. Phys.* **15**, 013061.
[34] Kobayashi, T., 2011 *et al. Plasma Phys. Control. Fusion* **53**, 095012.
[35] Luxon, J.L., 2002 *Nucl. Fusion* **42**, 614.
[36] Yakovlev, M. *et al.* 2005 *Phys. Plasmas* **12**, 092506.
[37] Inagaki, S., 2004 *et al. Phys. Rev. Lett.* **92**, 055002.
[38] Spakman, Q.W., *et al.* 2008 *Nucl. Fusion* **48** 115005.
[39] D′Angelo, F., and R.Paccagnella, 1996 *Phys. Plasmas* **3** 2353.
[40] Lorenzini, R., *et al.* 2009 *Nature Phys.* **5** 570 (2009).
[41] Bergerson, W.F., *et al.* 2011 *Phys. Rev. Lett.* **107** 255001.
[42] Ida, K., *et al.* 2015 *Sci. Rep.* **5** 16165.
[43] Evans, T.E. *et al.* 2014 "Comparative Studies of Static Edge Magnetic Islands in DIII-D and LHD", Proc. IAEA Fusion Energy Conf. EX/1-3.
[44] Scoville, J.T. and La Haye, R.J., 2003 *Nucl. Fusion* **43** 250.
[45] Ida, K., *et al.* 2015 *Plasma Phys. Control Fusion* **57** 014036.
[46] Ida, K., *et al.* 2012 *Phys. Rev. Lett.* **109** 065001.
[47] Ida, K., *et al.* 2015 *Nature Com.* **6**, 5816.
[48] Narushima, Y *et al.* 2015 *Nucl. Fusion* **55** 073004.
[49] Smolyakov, A.I., 1993 *Plasma Phys. Controlled Fusion* **35**, 657.
[50] Itoh, K., *et al..*, 2005 *Phys. Plasmas* **12**, 072512.
[51] Hahm, T.S. and Kulsrud, R.M., 1985 *Phys. Fluids* **28**, 2412.
[52] Fitzpatrick, R., 1995 *Phys. Plasmas* **2**, 825.
[53] Hahm, T.S., Diamond, P.H., Lin, Z., Itoh, K., and Itoh, S.-I., 2004 *Plasma Phys. Controlled Fusion* **46**, A323.
[54] Gurcan, O.D., Diamond, P.H., Hahm, T.S., Lin, Z., 2005 *Phys. Plasmas* **12** 032303.
[55] Ida, K., *et al.* 2008 *Phys. Rev. Lett.* **100** 045003.
[56] Ida, K., *et al.* 2001 *Phys. Rev. Lett.* **88** 015002.
[57] Isayama, A., *et al.* 1999 *Plasma Phys. Control. Fusion* **41** 35.
[58] Ida, K., *et al.* 2013 *Phys. Rev. Lett.* **111** 055001.
[59] Ida, K., *et al.* 2010 *Nucl. Fusion* **50**, 064007.
[60] Hidalgo, C., *et al.* 2002 *New J. Phys.* **4** 51.
[61] Diamond, P.H., Dupree, T.H., Tetreault, D.J., 1980 *Phys. Rev. Lett.* **45** 562.
[62] Liang, Y., *et al.* 2007 *Nucl. Fusion* **47** L21.
[63] Wesson, J.A., Gill, R.D., Hugon, M., *et al.* 1989 *Nucl. Fusion* **29** 641.
[64] Carreras, B., *et al.* 1980 *Phys. Fluids* **23** 1811.
[65] Evans, T.E., *et al.* 2006 *Nature Phys.* **2**, 419.
[66] Liang, Y.,*et al.* 2007 *Phys. Rev. Lett.* **98**, 265004.
[67] Suzuki, Y., *et al.* 2006 *Nucl. Fusion* **46** L19.
[68] Itagaki, M., *et al.* 2012 *Plasma Phys. Control. Fusion* **54** 125003.
[69] Suzuki, Y., *et al.* 2013 *Plasma Phys. Control. Fusion* **55** 124042.
[70] Ferraro, N.M., 2013 *et al. Nucl. Fusion* **53**, 073042.
[71] Lichtenberg, A. J., *et al.* 1992 *Nucl. Fusion* **32** 495.
[72] Itoh, K., *et al.* 1992 *Nucl. Fusion* **32** 1851.
[73] Terry, P.W. *et al.* 1996 *Phys. Plasmas* **3** 1999.
[74] Mahmood, A., Eriksson, A. and Weiland, J. 2010 *Phys. Plasmas* **17** 122310.
[75] Parker, E.N., 1963 *ApJS* **8** 177.
[76] Yokoyama, T. and Shibata, K. 1994 *ApJ* **436** L197.

[77] Shibata, K. and Tanuma, S., 2001 *Earth Planets Space*, **53** 473.
[78] Ida, K. *et al.* 2015 *Nucl. Fusion* **55** 013022.
[79] Ida, K. *et al.* 2015 *Nucl. Fusion* **55** 104018.
[80] Inagaki, S. *et al.* 2013 *Plasma Fusion Res.* **8** 1202172.
[81] Inagaki, S. *et al.* 2014 *Plasma Fusion Res.* **9** 1202052.
[82] Inagaki, S. *et al.* 2013 *Nucl. Fusion* **53** 113006.